

PACS numbers: 42.55.Lt; 81.65.Cf
DOI: 10.1070/QE2000v030n06ABEH001750

Surface oxide removal by a XeCl laser for decontamination

M L Sentis, Ph Delaporte, W Marine, O Uteza

Abstract. The laser ablation performed with an automated excimer XeCl laser unit is used for large surface cleaning. The study focuses on metal surfaces that are oxidised and are representative of contaminated surfaces with radionuclides in a context of nuclear power plant maintenance. The unit contains an XeCl laser, the beam delivery system, the particle collection cell, and the system for real-time control of cleaning processes. The interaction of laser radiation with a surface is considered, in particular, the surface damage caused by cleaning radiation. The beam delivery system consists of an optical fibre bundle of 5 m long and allows delivering 150 W at 308 nm for laser surface cleaning. The cleaning process is controlled by analysing in real time the plasma electric field evolution. The system permits the cleaning of 2 to 6 m^2 h^{-1} of oxides with only slight substrate modifications.

1. Introduction

Cleaning up and restoring to initial conditions the areas contaminated by different activities is now a priority not only for governments, but also for a variety of organisations responsible for contamination or having been hired to clean it up. Among environmental restoration activities, decontamination mainly concerns the removal of hazardous material (typically, radioactive) from facilities, soils or equipment usually by washing, chemical action or mechanical cleaning. This returns such sites, facilities or equipment to safe conditions for an additional use or possibly easier, less costly disposal.

Reducing radiation exposure among maintenance workers is a key element in operating and maintenance costs of nuclear plants. Although radiation fields reach a plateau after gradually rising through the early years (fuel cycles) of plant operation, plants may require more frequent maintenance as they age. At higher radiation field levels, more and larger crews are necessary, and limiting personnel radiation exposures (2 rem per year is the exposure limit for an individual set by the International Commission on Radiological Protection) constrains plant productivity. Crews cannot stay as long in a radiation control area, and setup and cleanup requirements are much greater than they would be for the same work in a nonradioactive environment.

Today, mechanical and chemical decontamination technologies are well developed and widely used. Mechanical decontamination methods are based on physically dislodging the surface contamination. Chemical decontamination includes methods that use chemical agents to loosen or solubilise the surface contamination. However, these techniques have some disadvantages: secondary waste streams that must be treated, a large volume of waste, significant splashing and spread of contamination if not controlled carefully, difficult to perform remotely, use of hazardous chemicals, and the fact that it is labor intensive.

Therefore, new decontamination technologies are needed that will minimize wastes and reduce radiation exposure for workers. They have to be performed in a manner that is safer, quicker, superior and thriftier. Laser processing offers a new range of opportunities and processing techniques for surface removal that can often overcome some of the current processing limitations. Lasers have been used extensively in surface processing: applying coatings, heat treating, and, as will be discussed below, surface cleaning.

In this paper, we considered general problems of laser surface cleaning and, specifically, the problems of using UV laser cleaning. We also demonstrate the potentialities of laser surface cleaning and describe the large area laser cleaning system under development.

2. Cleaning laser system

2.1 Choice of laser wavelength and pulse duration

Today, mainly three types of lasers are used as tools for industrial applications: CO_2 lasers ($\lambda = 10.6$ μm), Nd:YAG lasers ($\lambda = 1.06$ μm), and excimer lasers ($\lambda = 193$ to 351 nm). During laser material processing, in addition to the density of energy, two other laser parameters have a significant influence on the possible modifications of irradiated material – the wavelength λ and the duration τ of the laser pulse. Indeed, the thickness of the surface layer of the material which will be affected by the radiation is inversely proportional to the material absorption coefficient $\alpha(\lambda)$. For example for iron, $\alpha(\lambda)$ is $\sim 1\%$ for 10.6 μm, $\sim 20\%$ for 1.06 μm, and $\sim 50\%$ for 308 nm (XeCl excimer laser) [1]. The duration of the laser pulse influences the thickness of the thermally affected zone. This thickness is approximately proportional to the square root of the duration of the laser pulse. Thus, for a low thermal modification of substrates, as is it required for cleaning processes, the use of a short laser wavelength and a short pulse duration (i.e., nanoseconde range and below) is appropriate.

M L Sentis, Ph Delaporte, W Marine, O Uteza Laser Ablation and Applications Laboratory LP3 FRE 2165 6594 CNRS and GPEC UMR 6631 CNRS, Aix-Marseille II University, Campus de Luminy, case 918, 13288 Marseille, France

Received 20 December 1999
Kvantovaya Elektronika **30** (6) 495 – 500 (2000)
Submitted in English, edited by M N Sapozhnikov

If only the aspects of laser-matter interaction were to be taken into account in a decontamination system, a laser with a wavelength of 193 nm (ArF) and with a $\sim$ 10 ns pulse duration would be very well adapted. However, it is also necessary to consider the problem of the transport of the laser beam by optical fibres for the obvious reasons of automation and process safety. Unfortunately, a strong power radiation at 193 nm is currently not transmissible by optical fibre. Optical fibres that allow laser beam transmission of high power and short wavelength are made of silica. Taking into account the tramsmission characteristics of this material, the transmission of a radiation having a minimal wavelength of 308 mm (XeCl laser) is realistic today [2].

As a result, the choice of laser wavelength is a tradeoff between the possibility of achieving a laser beam delivery system by optical fibres, a high laser-matter coupling, and the lowest substrate residual laser damage. Nd:YAG laser is a possible candidate with a good optical fibre transmission [3], but its absorption coefficient is generally low for metals and its photon energy (i.e. 1.2 eV) is far beyond the bounding energy of most of oxides and metals. For this reson, a high density energy (more than 5 J cm^{-2}) is generally required to efficiently remove oxides inducing, unfortunately, thermal damage of the substrate.

The XeCl laser, at 308 nm, with a pulse duration of 50 to 200 ns represents a good compromise. In addition, this laser also presents the advantage of being well developed and available on the industrial market with a high average power (more than 500 W). The problem of UV light transmission through optical fibre is not yet completely solved, but as will be presented in the next section of this paper, operating conditions may be found to transmit high average power at 308 nm.

For the cleaning experiments developed in our laboratory, a high average power XeCl laser (CILAS 635) [4] has been used. The laser system is 2 m high, 1.3 m wide and 1.8 m long and its energetic characteristics are as follows: a pulse duration (FWHM) of 70 ns, an output energy maximum of 3 J, a repetition rate maximum of 500 Hz, and an average power of 1 kW at a repetition rate of 400 Hz.

2.2 Laser beam delivery

In order to optimise the transmission of high power excimer laser through silica fibres, the transmission behaviour of optical fibres under irradiation of XeCl laser has been studied. A spectroscopic study of the fibre core fluorescence during and after UV irradiation has been performed to characterise the colour centre formation. The optical fibres were also tested for different laser parameters, in order to determine the best laser operating conditions under which these fibres must be used for industrial applications. The fibres were step-index silica fibres (Polymicro 600/660/700μm). The 600-μm-diameter core is made of pure synthetic fused silica and a fluorine doped synthetic fused silica cladding. The typical OH content is 800 ppm, and numerical aperture of the fibres was 0.2.

Fibres with a length between 2 and 10 m were tested. The fibre transmission behaviour was studied by varying several laser parameters – number of shots, repetition rate, energy density, pulse duration. Fig. 1 shows, as an example, the transmission of a 2 m long fibre as a function of the number of laser pulses for three different laser repetition rates and for an energy density of 6 J cm^{-2}. In each case, the transmission reached a stable value after 2000 laser shots. This quantity is lower when the pulse repetition rate is increased. Indeed, at a high repetition rate, there is less time for colour centre bleaching.

The energy density E is also a laser parameter that influences the colour centre formation mechanism [5]. The fibre transmission T has been measured for different input energy densities and for a pulse repetition rate of 50 and 160 Hz. The same behaviour of T, as illustrated in Fig. 1, was observed. We determined the laser induced absorption coefficients after 10^4 shots when the saturation is reached. The linear dependence of $1/T$ on E, which was also observed in Refs [5–7], proves that colour centre formation results from two photon absorption.

The laser pulse duration also strongly affects the laser

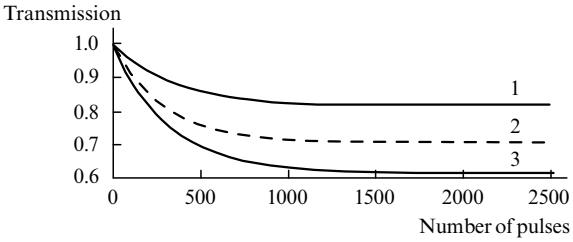

Figure 1. Fibre transmission as a function of the number of laser pulses for the energy density 6 J cm^{-2} and pulse repetition rates 10 (1), 50 (2), and 160 Hz (3).

induced absorption in the fibre core [8]. With a pulse duration of 70 ns, which is longer than that for usual commercial lasers (15 to 30 ns), the colour centre formation is reduced.

Thus, to transmit a high average power and keep an absorption in the fibre core as low as possible, the choice of a low energy density and a high repetition rate presents a good compromise. On this assumption, we tested a 90 fibre bundle of 5 m long. This choice of a large number of optical fibres permits one to reduce the energy transmitted into each fibre and the colour centre formation, and to transport a high average power at high frequency. The coupling efficiency, defined as the ratio between the total core fibre surface and the surface of the bundle on which the rectangular laser beam will arrive, was $\sim$ 72%.

At the output of the fibre bundle, two silica lenses were placed to shape the laser beam on the oxide surface. With an energy density of 3 J cm^{-2} at the entrance of the fibres and a pulse repetition rate of 300 Hz, the overall efficiency (coupling, transmission, and beam shaping) was $\sim$ 50%. The combination of these laser parameters results in one of the highest UV average power transmitted with fibre cables, since 150 W at 308 nm are directly available for surface processing with an optical fibre delivery system of 5 m long. This experiment has been running for one hour without any significant decrease in the transmitted average laser power.

2.3 Plasma expansion and ablated particle cell collection

During the interaction of a laser beam of a short wavelength (UV) with a short pulse duration, the photon energy is absorbed in a low thickness of material (skin depth $\sim \alpha^{-1}$), the laser power density deposited into the matter thus reaches values often higher than 1 GW mm^{-3}. Under these conditions, matter is ejected from the surface of material in the form of a plasma jet called 'plasma plume'. This plume is mainly composed of atoms and molecules in their ground, excited or ionized states. These particles initially move per-

pendicular to the material surface with velocities of about 10^5 cm s^{-1}. In the case of a surface irradiated in ambient air, expansion distance is ~ 2 to 10 mm, depending on the laser energy density. Thus, it is imperative to collect these ablated particles, which can either be redeposited on the sample surface (debris) or contaminate the surrounding atmosphere. A collecting cell is generally placed close to the surface to pick up all the particles of the plume.

To improve the collection of the contaminating particles, both experimental and modeling studies of the plasma expansion have been performed. For a multi-component substrate, like iron or stainless steel ablated in air, the physical processes are too complicated to be correctly modeled. For this reason, we studied a one-component Si target irradiated in noble gases (Ar or He).

Physical processes during laser ablation produced by short laser pulses (ranging from picoseconds to nanoseconds) and relatively low laser fluences (less than 10 J cm^{-2}, typical of cleaning conditions) can be described by three successive stages [9, 10]: (i) evaporation of the target material, (ii) interaction of the evaporated cloud with the laser beam, resulting in cloud heating and plasma formation, and (iii) plasma plume expansion into vacuum or background gas environment. The first two processes occur during the laser pulse. For nanosecond laser pulses, one can assume that the last process (i.e., expansion stage) starts after the laser pulse terminates and, thus, can be considered separately.

Plasma expansion into a vacuum environment is a simple adiabatic process that can be fully described by theoretical models and numerical gas dynamic simulations [9, 10]. Plasma upon its expansion into a background gas becomes considerably more complicated due to the development of new involved physical processes such as deceleration, formation of shock wave, thermal conduction, diffusion, recombination and clustering.

A deeper understanding of the plasma plume expansion has been gained combining experimental results with a multicomponent two-dimensional model developed at our laboratory. The three-dimensional axisymmetric Navier – Stokes equations for a compressible liquid were solved for a multi-component gas, including the effects of mass and forced diffusion, thermal conduction, and viscosity. These equations can be written in the form [11]

$$\frac{\partial \rho_i}{\partial t} + \operatorname{div}\left[\rho_i (v + v_{\mathrm{d}i})\right] = \omega_i\,, \quad i = 1, \ldots, 4\,, \tag{1}$$

$$\frac{\partial \rho v}{\partial t} + \operatorname{div}(\rho v v - p\mathbf{I} + \tilde{\tau}) = 0\,, \tag{2}$$

$$\frac{\partial E_{\mathrm{a}}}{\partial t} + \operatorname{div}\left(E_{\mathrm{a}} v - (-p_{\mathrm{a}}\mathbf{I} + \tilde{\tau})v + \boldsymbol{q}\right) = S_{\mathrm{a}}\,, \tag{3}$$

$$\frac{\partial E_{\mathrm{e}}}{\partial t} + \operatorname{div}\left[(E_{\mathrm{e}} + p_{\mathrm{e}})(v + v_{\mathrm{de}})\right] = S_{\mathrm{e}} + F_{\mathrm{e}}\,. \tag{4}$$

Here, ρ_i, $v_{\mathrm{d}i}$, ω_i are the density, the diffusion velocity, and mass source term of the ith component, respectively; v_{de} is the electron diffusion velocity; v is the velocity; ρ is the density of the mixture; p_{a} and p_{e} are the atom-ion and electron pressure, respectively; p is the overall pressure; $\tilde{\tau}$ is the viscous shear stress tensor; E_{a} and E_{e} are the atom-ion and electron energies, respectively; S_{a} and S_{e} are the atom-ion and electron energies source terms, respectively; I is the unity tensor; $i = 1$ corresponds to neutral atoms, $i = 2, 3$ – to ions and electrons, respectively, $i = 4$ – to the neutral ambient atoms.

A detailed description of the transport coefficients (thermal conductivity and viscosity of the individual Si, Ar and He gases, binary diffusion), which are expressed as polynomial functions of the temperature, can be found in [12]. This numerical study was confirmed by time-of-flight experiments with atoms and molecules and temperature measurements of their laser-induced fluorescence. This study permited to describe adequately the overall plasma expansion behaviour into a background gas, such as the mixing zone evolution, as well as the temperature and the density evolution of the plasma plume.

For surface cleaning, it is interesting to investigate the influence of background gas nature and pressure on the plasma expansion behaviour to improve the efficiency of the collecting cell. Fig. 2 shows, for example, the simulated Si density profile along the plume symmetry axis z at $t =$ 2.4 μs and for a laser fluence of 2.4 J cm^{-2}, with 400 and 700 mTorr of Ar. The increase in the Si density near the target surface ($z < 0.2$ mm) with increasing pressure of Ar indicates that Si atoms of the rarefied plume are efficiently driven by the backward-moving Ar gas as a result of mass diffusion. The backward motion of Si atoms becomes more significant with increasing Ar pressure. The splitting of the Si plume (i.e., two maximum density) is more pronounced with 700 mTorr of Ar than with the 400 mTorr (Fig. 2). The numerical results obtained are in good agreement with experimental results indicating a significant deposition increase of Si particles around the laser spot when the Ar pressure is increased [13].

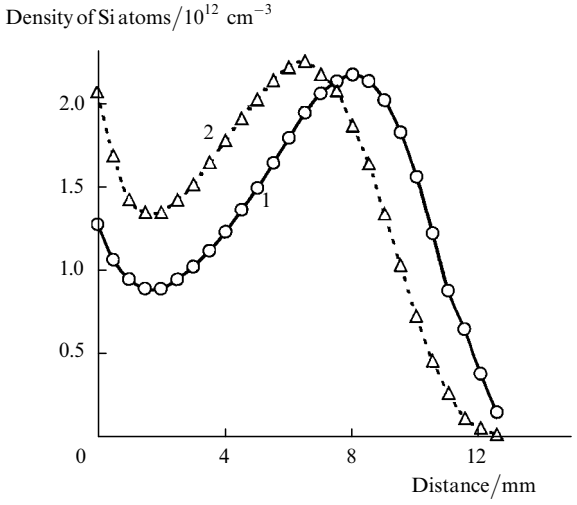

Figure 2. 2D Navier – Stokes gas-dynamic calculation of the Si density as a function of the distance from the surface at the moment $t = 2.4$ μs for an Ar pressure of 400 (1) and 700 mTorr (2) and the laser fluence of 2.4 J cm^{-2}.

Based on these studies, a coaxial nozzle was designed. It includes two lenses for laser beam shaping after the 90 fibre bundle and allows one to draw up the ablated particles with a flow speed of 10 to 100 m s^{-1}.

2.4 Real-time control of laser cleaning process

In order to protect workers against hazardous radiation and to reduce the cost of decontamination, automated efficient techniques have to be developed to control the decontami-

nation processes. Different techniques are available, such as remote viewing with a TV camera, acoustic noise detection, optical emission spectroscopy, etc. In the cleaning system under study, two approaches were used. The first one is based on optical emission spectroscopy, with the detection in real time of cesium line, for example. The second one, more original, is based on the detection and analysis of the laser plasma electric field.

We have studied [14] the possibility of measuring the electric field induced by a laser plasma using a rather simple probe method. We investigated the peculiarities of field generation upon the plasma production on different targets in order to control the decontamination of metal substrates.

The experiments were carried out for various targets placed in air at the ambient pressure ($p = 1$ atm). Samples of different metals (Fe, Cu, steel, etc.) were used as conductive targets, while samples of Teflon or oxides as dielectric ones. The potential of the electric field near the laser plasma was measured by an electric probe. The probe was a segment of a central conductor of a 50 Ohms impedance cable, 1 cm long and 0.4 mm in diameter, matched through the impedance of 50 Ohms to the input of a high frequency oscilloscope. The braid of the cable was grounded.

First, we found that the temporal shape and amplitude of the probe signal $U(t)$ during the plasma production depend on the presence of the metal grounded objects placed near the probe. The approach of these objects leads to a change in the shape of signals from the bipolar with the same areas under the positive and negative half waves to the unipolar ones. This change is explained by the increase in the probe capacitance caused by the adjacent metal. The experiments revealed the appearance of the electric potential U near the plasma plume starting from the threshold of the plasma initiation both on dielectric and conductive targets. The amplitude and shape of the signal U were independent of whether the probe was stripped or left in the dielectric insulator. Control experiments showed that this potential is not related to the photo-effect from the probe surface but is determined by the position of the probe with respect to the spatial position of the plasma electric field.

We found in our experiments that structures and magnitudes of electric potentials of laser plasma were substantially different for dielectric and conductive targets. Fig. 3 shows, for example, the dependence of the probe signal maximum on the number of laser pulses required to remove oxides from the surface of a piece made of iron. The experiment was done in air at the atmospheric pressure. After approximately 30 laser shots, the layer of oxides was totally removed and the ratio of signals from a surface with oxides and a cleaned surface was high enough (more than 20) to remote the decontamination process.

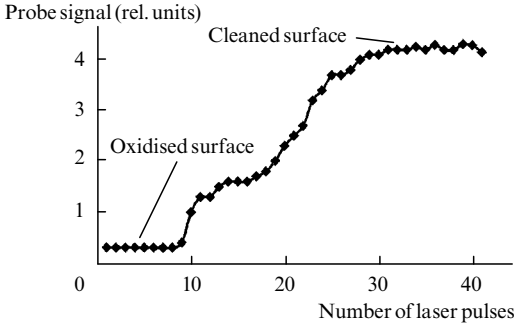

Figure 3. Electric field signal evolution during laser cleaning of oxides.

2.5 Laser decontamination unit

A demonstration decontamination unit was constructed on the basis of the elements described in the previous paragraphs. It included a XeCl laser CILAS 635, the 5 m long fibre delivery system, a robot, the collecting cell, a pump with a microparticle filter and a computer to control the system and the cleaning quality.

The robot employed to drive the collecting cell is a RX130 Stäubli, which is used in nuclear plants. The maximum speed of the robot arm was 1 m s^{-1}. Fig. 4 shows the arm of the robot supporting the collecting cell with the optical fibre delivery system and the suction duct.

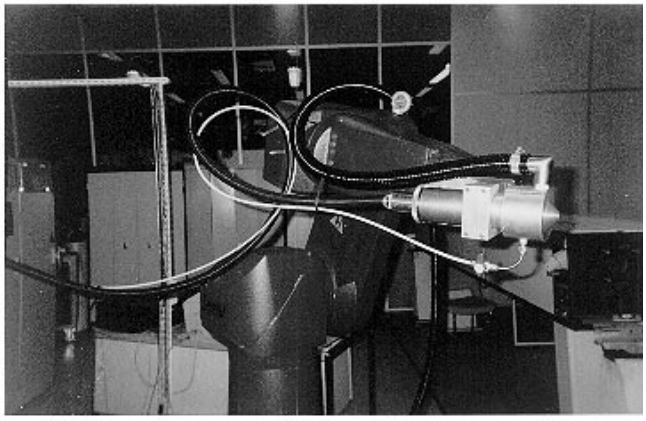

Figure 4. Picture of the demonstration decontamination unit.

3. Cleaning results

The first studies were devoted to the measurement of the damage threshold of stainless steel (304 and 316L) and the substrate modification induced by the XeCl laser. We observed no visual damage for a fluence less than 2 J cm^{-2} and an ablation threshold around 1 J cm^{-2}. Fig. 5 shows a Scanning Electron Microscopy (SEM) image of the surface of a stainless steel sample etched by 5 laser shots at a fluence of 2 J cm^{-2}. One can clearly see micro-cracks inherent to

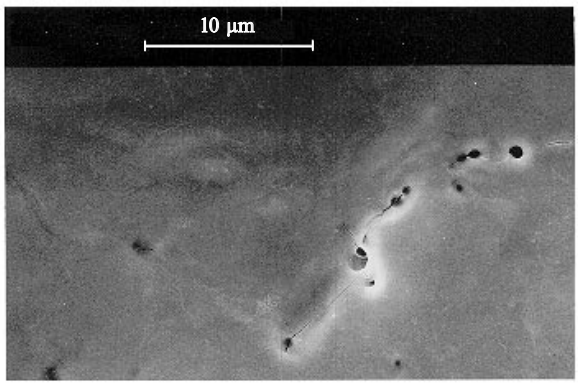

Figure 5. SEM image of a stainless steel surface after laser irradiation at 308 nm (five 2-J cm^{-2} laser shots).

such a material, which remain open after laser irradiation, showing that thermal processes like surface melting are negligible. The fact that a cleaning surface with an excimer laser does not cause the closure of micro-cracks is very favourable in the case of radioactive decontamination because radioactive elements generally migrate in fissures and are not definitively trapped in the substrate by such surface processing.

Fig. 6 shows two SEM images of an oxidized stainless steel sample before and after cleaning by four 1.5 J cm^{-2} laser pulses. After laser processing, oxides were completely removed and the surface was very smooth.

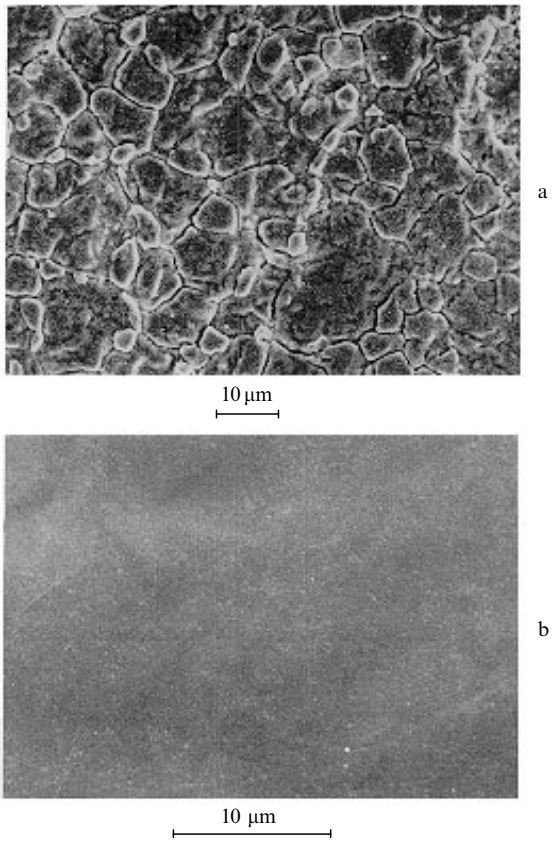

Figure 6. SEM images of an oxidized stainless steel sample before (a) and after (b) cleaning by four 1.5- J cm^{-2} laser pulses.

Fig. 7 presents SEM cross section images of a sample before and after laser cleaning by 100 6-J cm^{-2} laser pulses. No modifications of the substrate was detected; we only observed at the nanometer scale a slight thickening of the inherent oxide layer ($\sim$ 50 nm before irradiation (Fig. 7a) and $\sim$ 80 nm after (Fig.7c)). One may note that nanosecond UV laser ablation causes a very weak thermal effect even when a great number of high-power pulses is used. For ablation parameters that are typical for cleaning conditions (1 – 2 J cm^{-2} and 10 – 20 laser shots), SEM images revealed no modification of the surface being cleaned.

Another very important aspect of the laser decontamination is the efficient collection of all the particles. Fig. 8 presents two x-ray fluorescence spectra of a stainless steel sample contaminated by nonradioactive chlorine and cesium before laser processing and after processing by 2 J cm^{-2} laser pulses using a collecting cell. After laser surface cleaning, all the contaminants have been efficiently removed by laser ablation combined with the suction system.

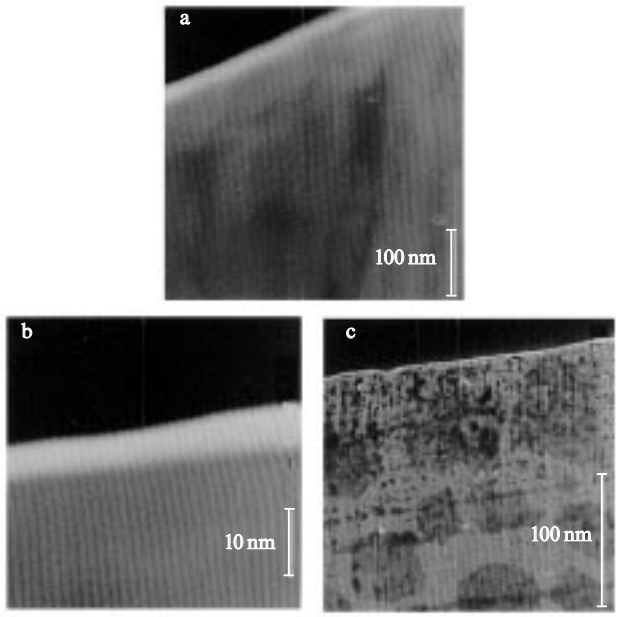

Figure 7. SEM cross section images of a sample before (a) and after (b) and (c) cleaning by one hundred 6-J cm^{-2} laser pulses.

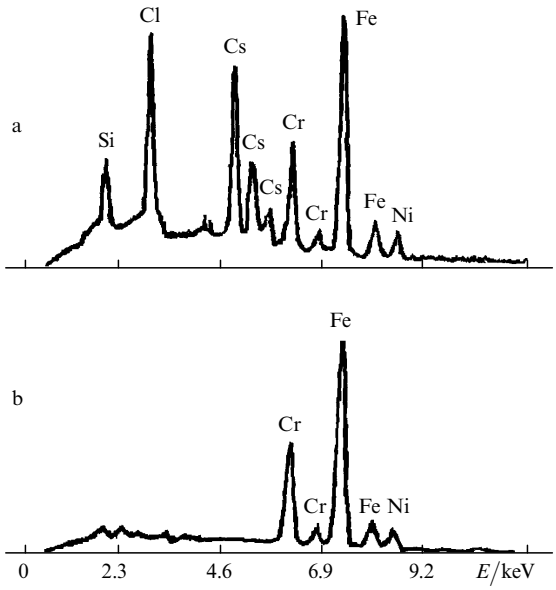

Figure 8. X-ray fluorescence spectra of a contaminated sample before (a) and after laser cleaning (b)

4. Conclusions

The laser decontamination system described above includes an XeCl laser (CILAS 635) and the robot arm (RX 130 Stäubli) with the remote control system and monitoring the degree of decontamination at an average power of 150 W at 308 nm with the 50% efficiency of delivering of laser radiation. The device provides efficient cleaning of surfaces without modification (or only slight modification) of the substrate.

This technique may be applied for cleaning of a large number of materials like metals, ceramics, glass, polymers, when contaminants are localised on the surface of the material. This decontamination unit provides cleaning of a surface with a scanning surface efficiency of 2 to 6 $m^2\ h^{-1}$, depending

on the type of contamination. The next experiments will be performed to validate the process for radioactive contamination.

Acknowledgements. This work was supported by ONET and ANVAR. The authors thank D Blin of ONET for his contribution in nuclear decontamination and his constant support and B Lacour of Cilas for his contribution to the excimer laser technology development.

References

1. Dausinger F, Shen J ISIJ International **33** 925 (1993)
2. Brimacombe R K, Taylor R S, Leopold K E J. Appl. Phys. **66** 4035 (1989)
3. Boechat A, Su D, Jones J D Meas. Sci. Technol. **2** 1107 (1991)
4. Lacour B, Brunet H, Besaucele H, Gagnol C, Vinent B Proc. SPIE **2206** 41 (1994.)
5. Hillrichs G, Dressel M, Hack H, Kunstamm R, Neu W I Appl. Phys. B **54** 208 (1992)
6. Artjushenko V G, Ikonov V, Pashinin V P, et al. Proc. SPIE **1420** 176 (1991)
7. Karlitschek P, Hillrichs G, Klein K F Optics Comm. **155** 376 (1998)
8. Taylor R S, Leopold K E, Mihailov S, Brimacombe R K Optics Comm. **63** 26 (1987)
9. Singh R K, Narayan J Phys. Rev. B **41** 8843 (1990)
10. Anisimov S I, Bäuerle D, Luk'yanchuck B Phys. Rev. B **48** 12076 (1993)
11. Oran E, Boris J P Numerical Simulation of Reactive Flow (New York, Elsevier 1987)
12. Kee R J, Dixon-Lewis G, Warnatz J, Coltrin M E, Miller J A Sandia Report SAND86-8246 (1986)
13. Movtchan I A, Marine W, Dreyfus R W, Le H C, Sentis M, Autric M Appl. Surf.Sci. **96 – 98** 251 (1996)
14. Kabashin A V, Nikitin P I, Marine W, Sentis M Kvantovaya Elektron. (Moscow) **25** 26 (1998) [Quantum Electronics **28** 24 (1998)]